Chemical Physics Letters 784 (2021) 139090

Contents lists available at ScienceDirect

Chemical Physics Letters

journal homepage: www.elsevier.com/locate/cplett

Research paper

Discovery of unusual morphological evolution of A-*graft*-(B-*block*-C) graft terpolymers by tuning the length of B component

Xu Zhang, Xiaoshan Fan *

State Key Laboratory for Modification of Chemical Fibers and Polymer Materials, College of Materials Science and Engineering, Innovation Center for Textile Science and Technology, Donghua University, Shanghai 201620, People's Republic of China

ARTICLE INFO

Keywords:
Self-consistent field theory
Self-assembly
Graft terpolymers
Multicompartment micelles
Entropy-driven morphological evolution

ABSTRACT

The self-assembly behaviors and morphological evolutions of the A-*g*-BC graft terpolymers in A-backbone-attractive solvents were examined by using the real-space implemented self-consistent field theory. The concentric structure-in-structure (B-*enwrap*-C) and surface-patched structure-on-structure (B-*patch*-C) multicompartment micelles were observed by tailoring the B block lengths. At longer length of B blocks, the A-*g*-BC graft terpolymers prefer to form the common concentric B-*enwrap*-C multicompartment micelles, while the B-*patch*-C multicompartment micelles with B patches on C surface favor the shorter length of B blocks. It was found that the formation of B-*patch*-C is driven by the conformational entropy of the B blocks. In addition, when the length of B block decreases into a much lower value, an unusual morphological evolution from raspberry-like to concentric multicompartment micelles was discovered, which was revealed to be driven by the conformational entropy of the inner blocks of A backbone between two adjacent graft points. The gained results could provide a deep insight into the mechanism behind the morphological evolution between concentric structure-in-structure (B-*enwrap*-C) and surface-patched structure-on-structure (B-*patch*-C) multicompartment micelles.

1. Introduction

Amphiphilic multiblock copolymers are capable of self-assembling into all sorts of complex multicompartment micelles in block-selective solvents, [1,2] such as segmented-worm-like, [3,4] toroidal or ring-shaped, [5,6] concentric or onion-like, [7,8] surface-patched structure-on-structure multicompartment micelles, [3,4,7] etc. Due to the great potential applications in the fields of biomedicine and nanotechnology, the multicompartment micelles have drawn considerable attention [8,9]. To date, the miktoarm star and linear multiblock copolymers have been found to be extensively studied for producing the multicompartment micelles with a variety of tunable nanostructures by tailoring the selectivity of solvents, [7,10,11] concentration, [6,12] length ratio of each block, [7,13–15] interactions between different components, [16] and so on. In addition to the nanoscale structures or morphologies, the self-assembly mechanisms of the formation and the morphological transformation of the obtained multicompartment micelles have been well documented [17–22]. In these aspects, the computer simulations and theoretical methods have been proven to be powerful tools for exploring the complex morphologies, which could provide more microscopic level information than the experimental observations, especially for the exploration of the self-assembly mechanism [5,7,10,11,13–16]. For example, Jiang et al. investigated the morphological evolution of multicompartment micelles from the self-assembly of linear "solvophilic-solvophobic-solvophobic" ABC triblock copolymers in A-selective solvents by using dissipative particle dynamics simulations, providing a deep insight into the mechanism behind the formation of raspberry-like and concentric multicompartment micelles as well as their morphological transformations [7].

In contrast with the well-concerned miktoarm star and linear multiblock copolymers, the graft copolymers are another kind of polymeric systems having the capacity of creating multicompartment micelles in selective solvents [23–28]. Recently, a novel kind of bottlebrush cellulose-*graft*-diblock copolymer thermoplastic elastomer (Cell-*g*-PBA-*b*-PMMA) was synthesized by Zhang et al. through grafting from cellulose backbones via surface-initiated atom transfer radical polymerization [29]. The cylindrical microphase-separated morphologies were observed for the solvent-cast film samples and the mechanical properties of the bottlebrush copolymer elastomers can be adjusted by controlling the block lengths and composition of the side chains [29]. In addition, it

* Corresponding author.
E-mail address: xsfan@dhu.edu.cn (X. Fan).

https://doi.org/10.1016/j.cplett.2021.139090
Received 24 August 2021; Received in revised form 26 September 2021; Accepted 27 September 2021
Available online 30 September 2021

is also confirmed that the as-prepared Cell-*g*-PBA-*b*-PMMA would be able to perfectly mimic the mechanical properties of human and animal skins which are essential to advance the future development of biomimetic polymer materials [30]. Inspired by the previous reports, in according to the formation principles of the multicompartment micelles, it can be convinced that the graft copolymers with backbone-*graft*-diblock architecture, i.e., A-*graft*-(B-*block*-C) or A-*g*-BC graft terpolymers, are promising candidates for forming multicompartment micelles in selective solvents. However, there is still few studies regarding the self-assembly behaviors of A-*g*-BC graft terpolymers into multicompartment micelles in selective solvents and the mechanism behind the formation of the multicompartment micelles are also unclear.

To evaluate the ability of A-*g*-BC graft terpolymers to self-assemble into multicompartment micelles and reveal the formation mechanism, in the present work, we performed the real-space implemented self-consistent field theory (SCFT) [31–33] to examine the self-assembly behaviors of A-*g*-BC graft terpolymers (shown in Fig. 1) in A-backbone-selective solvents, where the solvophobic BC diblock branches could take shape into the microphase-separated solvophobic cores. Two typical kinds of multicompartment micelles, including concentric structure-in-structure (B-*enwrap*-C) and surface-patched structure-on-structure (B-*patch*-C), were discovered at different lengths of B block. The formation of B-*patch*-C is proven to be driven by the conformational entropy of the B blocks. In addition, an unusual morphological evolution from raspberry-like to concentric B-*enwrap*-C multicompartment micelles was revealed to be an entropy-driven process corresponding to the inner blocks of A backbone between two adjacent graft points. The results gained through the SCFT calculations would provide an insight into the mechanism behind the morphological evolution between concentric B-*enwrap*-C and B-*patch*-C multicompartment micelles.

2. Theoretical model and method

We consider an incompressible polymeric solution system with total volume of V, containing n_P monodisperse and symmetric A-*g*-BC graft terpolymers in n_S A-selective solvents. As shown in Fig. 1, each A-*g*-BC graft terpolymer consists of one flexible A backbone along which are spaced m flexible BC diblock branches (denoted by G). The designed A-*g*-BC graft terpolymers are described as Gaussian chains with the same statistical segment length and fixed segment volume, denoted by a and ρ_0^{-1}, respectively. The statistical segment number of each A-*g*-BC graft terpolymer chain is $N = N_A + mN_G = N_A + m(N_B + N_C)$, where the N_A, N_G ($=N_B + N_C$), N_B, and N_C represent the statistical segment number of A backbone, BC diblock branch, B block in each BC diblock branch, and C block in each BC diblock branch per A-*g*-BC graft terpolymer chain, respectively. For convenience, the length ration of B block to BC diblock branch is defined as $\alpha = N_B/(N_B + N_C)$. For each A-*g*-BC graft terpolymer, the volume fraction of A, BC (G), B, and C blocks is $f_A = N_A/N$, $f_G = N_G/N$, $f_B = mN_B/N$, and $f_C = mN_C/N$, respectively. Therefore, $f_G = f_B + f_C$ and $\alpha = f_B/(f_B + f_C) = f_B/(1 - f_A)$. In the studied polymeric solution system, the concentration (i.e., volume fraction) of the A-*g*-BC graft terpolymers (denoted by P) and the solvent molecules (denoted by S) is c_P and $c_S = 1 - c_P$, respectively. The position where the ith junction point branched with BC diblock branch along the A backbone is located at τ_i and given by

$$\tau_i = \tau_1 + \frac{(i-1)(1-2\tau_1)}{m-1}, \quad 1 \leqslant i \leqslant m \tag{1}$$

where τ_1 is the first junction position spaced along the A backbone and is set to be $1/(m + 1)$.

In SCFT, the configuration of a single polymer chain is determined by a set of effective chemical potential fields, $\omega_I(\mathbf{r})$, to replace the actual interactions, where I = A, B, C, or S. The potential fields, $\omega_I(\mathbf{r})$, are conjugated to the density fields, $\phi_I(\mathbf{r})$. To ensure the incompressibility constraint ($\phi_A(\mathbf{r}) + \phi_B(\mathbf{r}) + \phi_C(\mathbf{r}) + \phi_S(\mathbf{r}) = 1$), the Lagrange multiplier $\xi(\mathbf{r})$ is introduced. The free energy density (in units of k_BT) of the solution system is expressed as

$$F = \frac{1}{V}\int dr \sum_{\substack{I,J=A,B,C,S \\ I\neq J}} \frac{1}{2}\chi_{IJ}N\phi_I(r)\phi_J(r) - \frac{1}{V}\int dr \sum_{I=A,B,C,S} \omega_I(r)\phi_I(r) - \frac{1}{V}\int dr\xi(r)[1 - \sum_{I=A,B,C,S}\phi_I(r)] - c_P\ln(\frac{Q_P}{V}) - Nc_S\ln(\frac{Q_S}{V}) \tag{2}$$

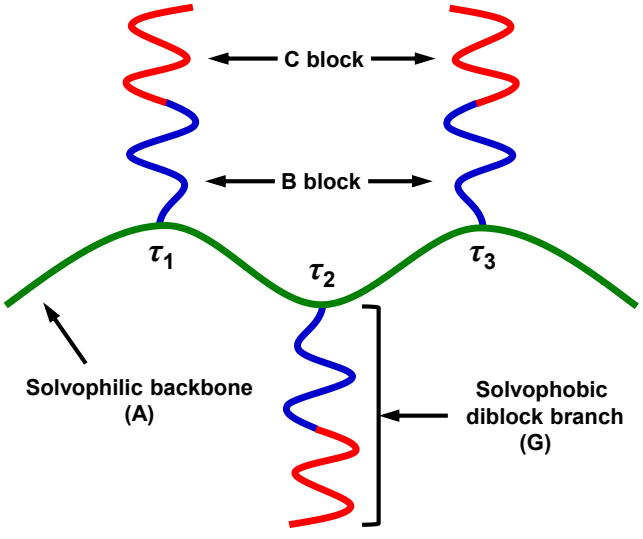

Fig. 1. Schematic presentation of A-*g*-BC graft terpolymer with $m = 3$ BC diblock branches (G) along the A backbone located at $\tau_1 = 1/(m + 1) = 0.25$, $\tau_2 = 0.50$, and $\tau_3 = 0.75$, respectively.

where k_B, T, and χ_{IJ} is the Boltzmann constant, absolute temperature, and Flory-Huggins interaction parameter between I and J species, respectively. The Q_P is the partition function of a single non-interacting A-*g*-BC graft terpolymer chain subject to the fields, $\omega_A(\mathbf{r})$, $\omega_B(\mathbf{r})$, and $\omega_C(\mathbf{r})$, in terms of the backbone propagator $q_A(\mathbf{r},s)$,

$$Q_P = \int dr q_A(\boldsymbol{r}, 1) \tag{3}$$

while the Q_S is the partition function of a solvent in the field, $\omega_S(\mathbf{r})$

$$Q_S = \int dr exp\left(-\frac{\omega_S(\boldsymbol{r})}{N}\right) \tag{4}$$

The spatial coordinate $\mathbf{r}$ is rescaled by R_g, where $R_g^2 = a^2N/6$.

The propagator of flexible A backbone can be divided into $m + 1$ segments according to the branched junctions of the BC diblock branches and is given by

$$q_A(r,s) = q_{A,i}(r,s) \tag{5}$$

The $q_{A,i}(\mathbf{r},s)$ represents the backbone propagator of the ith segment between $s = \tau_i$ and $s = \tau_{i+1}$, where s is the contour length subject to $\tau_i \leq s < \tau_{i+1}$ for $i = 0, 1, \ldots, m$. In particular, the $\tau_0 \equiv 0$ and $\tau_{m+1} \equiv 1$ is the position of the A backbone at the beginning and terminal free end, respectively. Each segment of the backbone propagator meets the

modified diffusion equation

$$\frac{N}{N_A}\frac{\partial q_{A,i}(\boldsymbol{r},s)}{\partial s} = \left[R_g^2\nabla^2 - \omega_A(\boldsymbol{r})\right]q_{A,i}(\boldsymbol{r},s) \tag{6}$$

subject to the following two initial conditions

$$q_{A,i}(\boldsymbol{r},\tau_i) = q_{A,i-1}(\boldsymbol{r},\tau_i^-)q_G(\boldsymbol{r},1), \quad i = 1,2,3,\cdots,m \tag{7}$$

$$q_{A,0}(\boldsymbol{r},0) = 1 \tag{8}$$

where $q_{A,i\text{-}1}(\mathbf{r},\tau_i^-)$ is the limit of the function when the contour length s approaches to τ_i from below (just after the junction point). The $q_G(\mathbf{r},s)$ is the propagator for the BC diblock branches satisfying the following modified diffusion equation

$$\frac{N}{N_G}\frac{\partial q_G(\boldsymbol{r},s)}{\partial s} = \left[R_g^2\nabla^2 - \omega_I(\boldsymbol{r})\right]q_G(\boldsymbol{r},s), \quad I = \begin{cases} C \text{ if } 0 < s \leqslant 1-\alpha \\ B \text{ if } 1-\alpha < s \leqslant 1 \end{cases} \tag{9}$$

subject to the initial condition $q_G(\mathbf{r},0) = 1$ at $s = 0$ for the free end of the BC diblock branches. The backward propagator, $q_{G,i}^{+}(\mathbf{r},s)$, of each BC-branch attached to the ith junction point is also defined and satisfies

$$\frac{N}{N_G}\frac{\partial q_{G,i}^{+}(\boldsymbol{r},s)}{\partial s} = \left[R_g^2\nabla^2 - \omega_I(\boldsymbol{r})\right]q_{G,i}^{+}(\boldsymbol{r},s), \quad I = \begin{cases} B \text{ if } 0 < s \leqslant \alpha \\ C \text{ if } \alpha < s \leqslant 1 \end{cases} \tag{10}$$

starting at the end of the BC diblock branch tethered to the A backbone. The initial condition of $q_{G,i}^{+}(\mathbf{r},s)$ is the product of the propagator and backward propagator of the backbone approaching to the ith junction point, satisfying

$$q_{G,i}^{+}(\boldsymbol{r},0) = q_{A,i-1}(\boldsymbol{r},\tau_i^-)q_{A,m-i-1}(\boldsymbol{r},(1-\tau_i)^-) = \frac{q_{A,i}(\boldsymbol{r},\tau_i)\,q_{A,m-i}(\boldsymbol{r},1-\tau_i)}{q_G^2(\boldsymbol{r},1)} \tag{11}$$

In conformity to the propagators and partition functions, the segment volume fractions or densities, $\phi_A(\mathbf{r})$, $\phi_B(\mathbf{r})$, $\phi_C(\mathbf{r})$, and $\phi_S(\mathbf{r})$, follow the following equation set

$$\phi_A(\boldsymbol{r}) = \frac{f_A c_P V}{Q_P}\sum_{i=0}^{m}\int_{\tau_i}^{\tau_{i+1}} ds q_{A,i}(\boldsymbol{r},s)q_{A,m-i}(\boldsymbol{r},1-s) \tag{12}$$

$$\phi_B(\boldsymbol{r}) = \frac{f_G c_P V}{Q_P}\sum_{i=1}^{m}\int_{\alpha}^{1} ds q_G(\boldsymbol{r},s)q_{G,i}^{+}(\boldsymbol{r},1-s) \tag{13}$$

$$\phi_C(\boldsymbol{r}) = \frac{f_G c_P V}{Q_P}\sum_{i=1}^{m}\int_{0}^{\alpha} ds q_G(\boldsymbol{r},s)q_{G,i}^{+}(\boldsymbol{r},1-s) \tag{14}$$

$$\phi_S(\boldsymbol{r}) = \frac{c_S V}{Q_S} exp\left(-\frac{\omega_S(\boldsymbol{r})}{N}\right) \tag{15}$$

Finally, the mean-field equations are achieved by minimizing the free energy with respect to $\phi_A(\mathbf{r})$, $\phi_B(\mathbf{r})$, $\phi_C(\mathbf{r})$, $\phi_S(\mathbf{r})$, and $\xi(\mathbf{r})$, as given by

$$\omega_A(\boldsymbol{r}) = \chi_{AB}N\phi_B(\boldsymbol{r}) + \chi_{AC}N\phi_C(\boldsymbol{r}) + \chi_{AS}N\phi_S(\boldsymbol{r}) + \xi(\boldsymbol{r}) \tag{16}$$

$$\omega_B(\boldsymbol{r}) = \chi_{AB}N\phi_A(\boldsymbol{r}) + \chi_{BC}N\phi_C(\boldsymbol{r}) + \chi_{BS}N\phi_S(\boldsymbol{r}) + \xi(\boldsymbol{r}) \tag{17}$$

$$\omega_C(\boldsymbol{r}) = \chi_{AC}N\phi_A(\boldsymbol{r}) + \chi_{BC}N\phi_B(\boldsymbol{r}) + \chi_{CS}N\phi_S(\boldsymbol{r}) + \xi(\boldsymbol{r}) \tag{18}$$

$$\omega_S(\boldsymbol{r}) = \chi_{AS}N\phi_A(\boldsymbol{r}) + \chi_{BS}N\phi_B(\boldsymbol{r}) + \chi_{CS}N\phi_C(\boldsymbol{r}) + \xi(\boldsymbol{r}) \tag{19}$$

$$\phi_A(\boldsymbol{r}) + \phi_B(\boldsymbol{r}) + \phi_C(\boldsymbol{r}) + \phi_S(\boldsymbol{r}) = 1 \tag{20}$$

The free energy can be split into the enthalpy (ΔU) and entropy ($-T\Delta S$) contribution, i.e., $\Delta F = \Delta U - T\Delta S$, which could be gained from Eq. (2), as expressed by

$$\Delta U = \frac{1}{2V}\int d\boldsymbol{r}\sum_{\substack{I,J=A,B,C,S \\ I\neq J}}\chi_{IJ}N\phi_I(\boldsymbol{r})\phi_J(\boldsymbol{r}) \tag{21}$$

$$\begin{aligned} -T\Delta S = & -\frac{1}{V}\int d\boldsymbol{r}\sum_{I=A,B,C,S}\omega_I(\boldsymbol{r})\phi_I(\boldsymbol{r}) \\ & -\frac{1}{V}\int d\boldsymbol{r}\xi(\boldsymbol{r})\left[1-\sum_{I=A,B,C,S}\phi_I(\boldsymbol{r})\right] \\ & -c_P ln\left(\frac{Q_P}{V}\right) - Nc_S ln\left(\frac{Q_S}{V}\right) \end{aligned} \tag{22}$$

The present simulations were carried out in the three-dimensional boxes with periodic boundary conditions, where the spatial resolutions were taken as $\Delta x < 0.1R_g$ and the contour step sizes were set to be $\Delta s = 0.01$. The numerical solution of the mean-field equations was started from a random initial state. The modified diffusion equations were solved *via* the pseudo-spectral method and operator splitting formula scheme. In the SCFT calculations, the numerical simulations proceeded until the relative accuracy in the fields (measured by $\sqrt{\sum_I\int\left[\omega_I^{new}(\boldsymbol{r}) - \omega_I^{old}(\boldsymbol{r})\right]^2 d\boldsymbol{r}/\sum_I\int d\boldsymbol{r}}$) is smaller than 10^{-6} and the incompressibility condition was achieved.

3. Results and discussion

The purpose of the present work is to get insight into the ability of A-*g*-BC graft terpolymers to self-assemble into multicompartment micelles in A-backbone-selective solvents. The examined A-*g*-BC graft terpolymers ($N = 40$) are frustrated with $\chi_{AB}N/m = \chi_{BC}N/m = 40$ and $\chi_{AC}N/m = 20$ consisting of the solvophilic backbone (A) and the solvophobic BC diblock branches by setting $\chi_{AS}N/m = 0$ and $\chi_{BS}N/m = \chi_{CS}N/m = 40$, in which the A backbone prefers to form the outermost coronas of the self-assembled multicompartment micelles. For simplicity and without loss of generality, the volume fraction of solvophilic A backbone in each A-*g*-BC graft terpolymer chain and the number of BC diblock branches along the A backbone is fixed as $f_A = 0.50$ ($f_B + f_C = 0.50$) and $m = 3$ with $\tau_1 = 1/(m+1) = 0.25$, respectively. The concentration of A-*g*-BC graft terpolymers in the solution is set to be $c_P = 0.10$. Therefore, the f_B is the only one variable parameter to be studied in the present work.

3.1. Effect of f_B on multicompartment micelles

Fig. 2 shows serval typical multicompartment micelles self-assembled from A-*g*-BC graft terpolymers in A-backbone-selective solvents (i.e., $\chi_{AS}N/m = 0$ and $\chi_{BS}N/m = \chi_{CS}N/m = 40$) varying in the B block length. For clarity, the solvents are omitted in all of the figures. At relative longer B blocks, the A-*g*-BC graft terpolymers prefer to form concentric structures-in-structure (B-*enwrap*-C) micelles, i.e., the core–shell-corona micelles, where the end solvophobic C blocks self-assemble into the innermost spherical C cores while the middle solvophobic B blocks form the shell enwrapping the spherical C cores, as illustrate in Fig. 2a ($f_B = 0.36$). Here, we designated this concentric structure-in-structure multicompartment micelles as **SSS**, where **S** (sphere), **S**, and **S** represent the structures of the whole scale, B rich domain, and C rich domain, respectively. The designation of the other multicompartment micelles also follows this rule.

As the f_B decreases, the middle B shells of the multicompartment micelles become perforated shells (denoted by **P**) patched on the surface of C cores due to the lower volume fraction of the B rich domains, leading to the self-assembly of C blocks into a bumped sphere (like a regular tetrahedron shape, denoted by **B**). This surface-patched structure-on-structure (B-*patch*-C) multicompartment micelles were designed as **SPB**, as shown in Fig. 2b ($f_B = 0.32$). With further shortening the length of B blocks, the pore size of the perforated shells self-assembled from the B blocks become larger or even separated into many small pieces of patch attached on the surface of C cores, while the structure of the C core would be changed accordingly. When the length of B and C blocks is equal (i.e., $f_B = f_C = 0.25$ in Fig. 2c), the middle solvophobic B blocks favor the separated patches stick to the outer surface of C cores

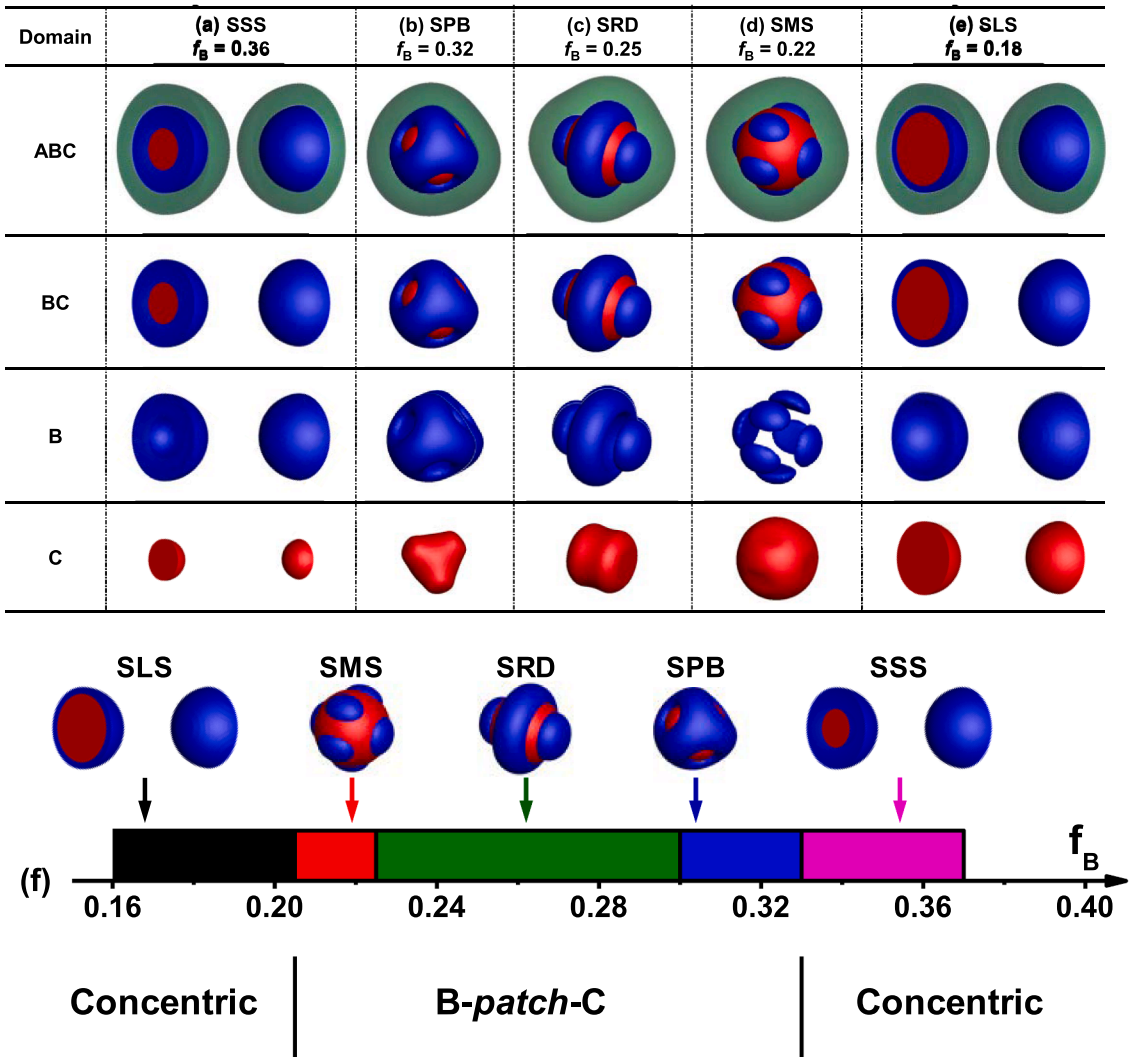

Fig. 2. Multicompartment micelles self-assembled from A-*g*-BC graft terpolymers in A-backbone-selective solvents ($\chi_{AS}N/m = 0$, $\chi_{BS}N/m = \chi_{CS}N/m = 40$, and $c_P = 0.10$) at (a) $f_B = 0.36$, (b) $f_B = 0.32$, (c) $f_B = 0.25$, (d) $f_B = 0.22$, and (e) $f_B = 0.18$ with $m = 3$, $\tau_1 = 0.25$, $f_A = 0.50$, $\chi_{AB}N/m = \chi_{BC}N/m = \chi_{BS}N/m = \chi_{CS}N/m = 40$, and $\chi_{AC}N/m = 20$. (f) One-dimensional diagram for the observed multicompartment micelles of (a-e). The solvent rich domains are omitted.

including two small semi-spherical structures and one ring structure (denoted by **R**), while the end solvophobic C blocks self-assemble into the innermost dumbbell-shaped cores (denoted by **D**) because of the structural constraint of ring-like patch [34]. This surface-patched structure-on-structure (B-*patch*-C) multicompartment micelles are designated as **SRD**, which possesses a UFO-like solvophobic BC cores, as shown in Fig. 2c.

Continuously decreasing the f_B, the ring patch of B domains separates into multiple small pieces of patch or semi-spheres (denoted by **M**) on the surface of the spherical C cores, leading to the patches-on-sphere multicompartment micelles, **SMS**, as illustrated in Fig. 2d ($f_B = 0.22$), which is also called raspberry-like multicompartment micelles in the previous study on the self-assembly of linear ABC triblock copolymers in A-selective solvents [7]. A more interesting phenomenon is that the concentric B-*enwrap*-C multicompartment micelles with thinner B shell could be observed at relative shorter length of B blocks, e.g., $f_B = 0.18$ as presented in Fig. 2e. The difference between the **SSS** multicompartment micelles self-assembled from A-*g*-BC graft terpolymers with relative longer (Fig. 2a) and shorter (Fig. 2e) B blocks is the thickness of the B shell and the size (or diameter) of the spherical C core, in which the longer B blocks correspond to the thicker B shells and smaller C cores, and vice versa. To distinguish from the **SSS** multicompartment micelles with thicker B shell (Fig. 2a, $f_B = 0.36$), these concentric B-*enwrap*-C multicompartment micelles with thinner B shell are designated as **SLS**, where the **L** denotes the thin-layer-like B rich domains.

To get more deep insight into the morphological evolution from the self-assembly of A-*g*-BC graft terpolymers in A-backbone-selective solvents by changing the length of B blocks, the observed multicompartment micelles were summarized into a one-dimensional diagram of morphology-f_B, which was shown in Fig. 2f. It is apparent from Fig. 2 that the morphologies of the multicompartment micelles undergo from concentric B-*enwrap*-C (**SSS** in Fig. 2a) to B-*patch*-C multicompartment micelles (**SPB** in Fig. 2b, **SRD** in Fig. 2c, and **SMS** in Fig. 2d) and then finally back to concentric B-*enwrap*-C multicompartment micelles (**SLS** in Fig. 2e) as the length of B blocks decreases. The formation of B-*patch*-C multicompartment micelles at shorter length of B blocks is due to the fact that the B blocks could not enwrap the C cores sufficiently. If the structures of the self-assembled multicompartment micelles still remain the concentric B-*enwrap*-C structures at shorter length of B blocks, the B shells should become thinner and be more stretched to make sure of completely covering the surface of C cores, which would give rise to a significant increase in free energy. To effectively moderate the thinner B shells and the stretching of B blocks, the B blocks are restricted to the patches on the surface of C cores. In addition, the structures of B-*patch*-C multicompartment micelles at shorter length of B blocks (**SPB** in Fig. 2b, **SRD** in Fig. 2c, and **SMS** in Fig. 2d) simultaneously introduce the A/C

interfaces and reduce the B/C interface areas, which is favorable to the interaction energy because of the frustrated interaction parameters ($\chi_{AC}N/m = 20 < \chi_{AB}N/m = \chi_{BC}N/m = 40$).

The similar morphological transformation from concentric (B-*enwrap*-C) to raspberry-like (B-*patch*-C) aggregates for the linear solvophilic-solvophobic-solvophobic ABC triblock terpolymers in A-selective solvents was also observed by Jiang et al. and concluded to an entropy-dominated process [7]. In the present work, a more interesting phenomenon is the morphological evolution from raspberry-like (B-*patch*-C) (**SMS** in Fig. 2d) to concentric (B-*enwrap*-C) multicompartment micelles with thinner B shells and larger C spheres (**SLS** in Fig. 2e) by decreasing the length of B blocks, which is totally different from or even opposite to the linear ABC triblock terpolymers. The formation of the concentric (B-*enwrap*-C) multicompartment micelles (**SLS**) at very short length of B block as well as the mechanism behind the morphological transformation is worth of being revealed and would be explained in detail in the later subsection.

3.2. Mechanism behind morphological evolution

In order to further clarify the effect of B block length on the morphological transformation between concentric B-*enwrap*-C and B-*patch*-C multicompartment micelles, the variation of free energy as a function of f_B upon the formation of the observed multicompartment micelles was further analyzed and presented in Fig. 3. As can be seen from the combination of Fig. 2f and Fig. 3, the surface-patched structure-on-structure multicompartment micelles (**SMS**, **SRD**, and **SPB**) are shown to be more stable than the concentric structure-in-structure multicompartment micelles (**SSS** and **SLS**) at the intermediate f_B. In addition, the **SRD** multicompartment micelles (as shown in Fig. 2c) have a large stable region from $f_B = 0.225$ to $f_B = 0.300$, while the other two surface-patched structure-on-structure multicompartment micelles (**SMS** and **SPB**) can only be stable in a very narrow region: $0.205 < f_B < 0.225$ for **SMS** and $0.305 < f_B < 0.325$ for **SPB**. There is nothing remarkable about the morphological evolution from concentric structure-in-structure to surface-patched structure-on-structure multicompartment micelles (**SSS** → **SPB** → **SRD** → **SMS**) with decreasing the f_B, which have been explained to be driven by the conformation entropy of B blocks similar to the self-assembly of linear ABC triblock terpolymers in A-selective solvents [7]. The unusual morphological evolution is the morphological transformation from raspberry-like (B-*patch*-C) to concentric (B-*enwrap*-C) multicompartment micelles (**SMS** → **SLS**) by shortening the f_B when the value of f_B is much lower, which is not yet discovered in the self-assembly of linear ABC triblock terpolymers in A-selective solvents.

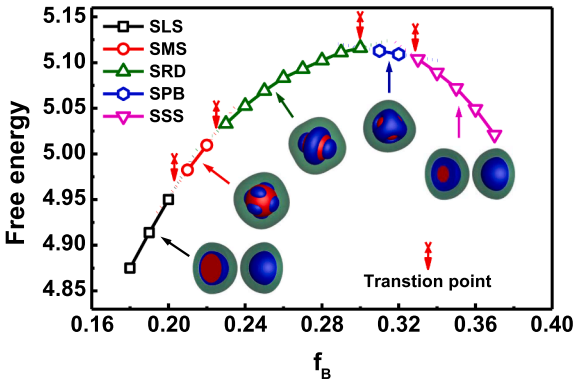

Fig. 3. Plots of free energy as a function of f_B for the observed multicompartment micelles. The transition points between two different adjacent structures are indicated by red arrows started with cross. The dot line is the extrapolation of the corresponding curve in order to obtain the intersection point (i.e., transition point).

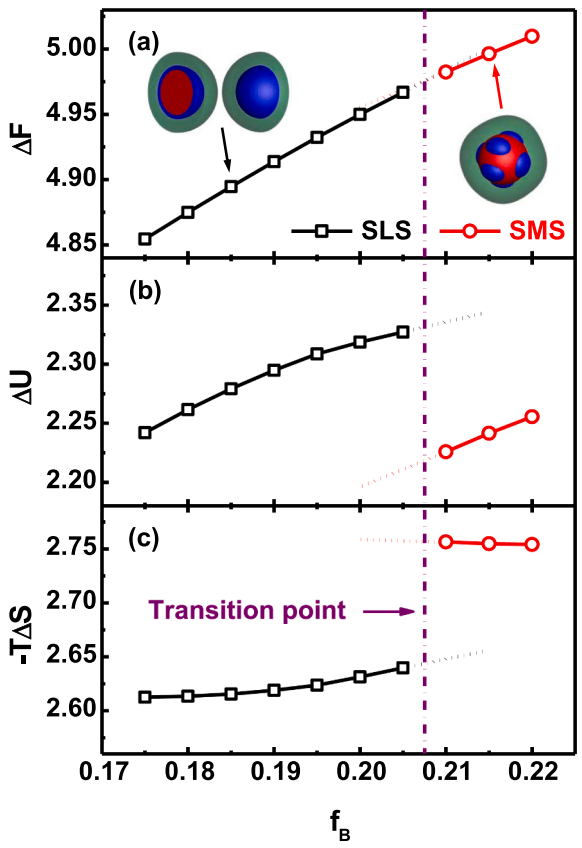

Fig. 4. (a) Free energy (ΔF), (b) interaction enthalpy (ΔU), and (c) conformational entropy ($-T\Delta S$) of the observed concentric (**SLS**) and raspberry-like (**SMS**) multicompartment micelles as a function of f_B. The morphological structure of **SLS** and **SMS** is shown in the left and right inset, respectively. The morphological transition point of **SLS**-**SMS** is indicated by a vertical short-dash dot line at $f_B = 0.2075$. The dot line is the extrapolation of the corresponding curve.

We further analyze the changes of the free energy (ΔF), interaction enthalpy (ΔU), and conformational entropy ($-T\Delta S$) of the observed **SMS** and **SLS** in more details upon decreasing the f_B to reveal the mechanism behind the morphological evolution of **SMS** → **SLS**, as presented in Fig. 4. For the raspberry-like multicompartment micelles (**SMS**), the interaction enthalpy (ΔU) decreases as the f_B decreases, while the conformational entropy ($-T\Delta S$) shows a slight increase. Upon the morphological transformation from raspberry-like (**SMS**) to concentric (**SLS**) multicompartment micelles, the interaction enthalpy (ΔU) jumps upwards to a much larger value, while the conformational entropy ($-T\Delta S$) drops down to a much lower value, indicating that the morphological transition of **SMS**-to-**SLS** as the f_B decreases is an entropy-driven process by sacrificing the interaction enthalpy.

In according to the above free energy analyses, a scheme was further provided to address the morphological transformation of **SMS**-to-**SLS** as the f_B decreases, as illustrated in Fig. 5. As indicated in Fig. 5a, the A backbone of the A-*g*-BC graft terpolymers can be divided into the free end and inner blocks according to the branched positions of the BC diblock branches (τ_1, τ_2, and τ_3). In the raspberry-like multicompartment micelles (**SMS**), not only could the inner blocks be the looped conformations, but also form the bridged conformations to bridge the two adjacent separated B patches, as illustrated in Fig. 5b. As the f_B decreases, the patches formed by B blocks would reduce which narrows the space for B blocks. Due to the fixed length of BC diblock branches ($f_B + f_C = 0.50$), the f_C increases as the f_B decreases, inducing the larger spherical C cores. Consequently, the distance between two adjacent separated B patches (denoted by d_B, as indicated in Fig. 5b) increases. If

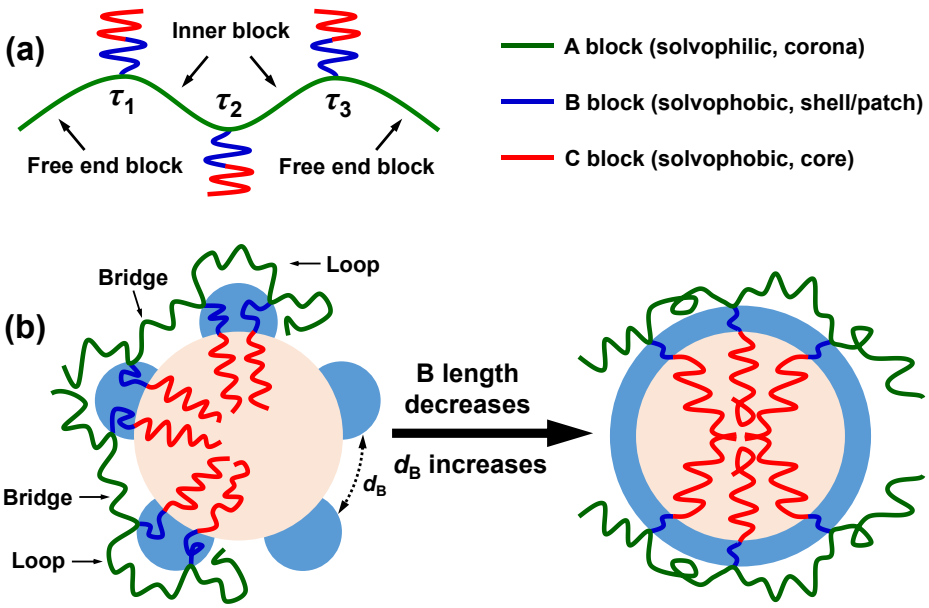

Fig. 5. (a) Schematic sketch of the free end and inner blocks for the A backbone of A-*g*-BC graft terpolymer chain. (b) Possible conformation of A-*g*-BC graft terpolymer chains (partly) in the raspberry-like (**SMS**) and concentric (**SLS**) multicompartment micelles. The light blue and yellow region represent the solvophobic domain formed by B and C blocks, respectively.

the self-assembled structures keep raspberry-like at shorter B block lengths, the bridged conformations of the inner blocks should be severely stretched to bridge the two adjacent separated B patches with larger distance (d_B), leading to a significant loss of conformational entropy of the bridged inner blocks. To relieve the elongation of the inner blocks, the concentric structure-in-structure (B-*enwrap*-C) multicompartment micelles (**SLS**) are then favored by sacrificing the conformational entropy of the shorter B blocks and the interaction enthalpy (Fig. 4b). Therefore, the morphological evolution from raspberry-like (**SMS**) to concentric (**SLS**) multicompartment micelles is driven by the conformational entropy of the inner blocks.

Unfortunately, there are no directly experimental restuls of multicompartment micelles self-assembled from A-*graft*-(B-*block*-C) terpolymers till now. Even so, the similar morphological evolutions based on A-*block*-(B-*graft*-C) terpolymers have been experimentally observed, which seem in agreement with the simulation results. Wu et al. have reported a simple but effective method for preparing various multi-compartment micelles: poly(styrene-*b*-4-vinylbenzyl triazolylmethyl methylthymine) (PS-*b*-PVBT) diblock copolymers blended with the adenine-terminated poly(ethylene oxide) (A-PEO) homopolymer to obtain pseudo A-*block*-(B-*graft*-C)-type terpolymers stabilized through thymine-adenine (T-A) multiple hydrogen bonding interactions between PVBT and A-PEO segments in DMF (N,N-dimethylformamide) common solvent after the addition of H_2O or MeCN selective solvent [23]. The transmission electron microscopy revealed several different multi-compartment micelle structures, including raspberry-like spheres (**SMS** in Fig. 2d), core–shell-corona spheres (**SSS** in Fig. 2a or **SLS** in Fig. 2e), core–shell-corona cylinders, nanostructured vesicles, onion-like structures (**SSS** in Fig. 2a or **SLS** in Fig. 2e), segmented worm-like cylinders, and woodlouse-like structures (**SPB** in Fig. 2b or **SRD** in Fig. 2c), upon varying the molecular weight of the PS-*b*-PVBT block segments and the concentration of the selective solvent. The structural changes in the multicompartment micelles could be induced, similar to those of ABC miktoarm star terpolymers, through simple blending of PS-*b*-PVBT block copolymers with an A-PEO homopolymer.

Overall, our results discovered the self-assembly behaviors and the morphological evolutions of the A-*g*-BC graft terpolymers in A-backbone-selective solvents by the real-space implemented self-consistent field theory, where the two different entropy-driven processes of the morphology transformation from B-*enwrap*-C to B-*patch*-C and B-*patch*-C to B-*enwrap*-C were revealed. However, it still remains plenty of rooms for further discovery both in the molecular and interaction parameters, including the effect of the molecular architecture parameters of the A-*g*-BC graft terpolymers (the number of BC diblock branches, the distribution of junction points, the length ratio of backbone to branch, etc.), the interaction strength between backbone and branch, the selectivity of solvents on the self-assembly behaviors as well the morphological evolution of the A-*g*-BC graft terpolymers in dilute solution, which is worthy of concerning in the future to provide more useful information for preparation and control of the complex multicompartment micelles.

4. Conclusions

We employed the real-space implemented self-consistent field theory to investigate the self-assembly behaviors and the morphological evolutions of the A-*g*-BC graft terpolymers in A-backbone-attractive solvents, where the two typical aggregates of concentric structure-in-structure (B-*enwrap*-C) and surface-patched structure-on-structure (B-*patch*-C) multicompartment micelles were observed by varying in the B block lengths. The A-*g*-BC graft terpolymers favor the common concentric B-*enwrap*-C multicompartment micelles at the longer B block lengths, while the multicompartment micelles with B patches on C surface (B-*patch*-C) at the shorter length of B blocks. The formation of B-*patch*-C multicompartment micelles has been proven to be driven by the conformational entropy of the B blocks. When the length of B blocks is much shorter than the C blocks, an unusual morphological transformation from raspberry-like (B-*patch*-C) to concentric (B-*enwrap*-C) multicompartment micelles was discovered, which was further revealed to being driven by the conformational entropy of the inner blocks of the A-*g*-BC graft terpolymer backbone. The gained results could provide useful information for regulating and controlling the fascinating self-assembly behaviors as well as the complex multicompartment micelles.

CRediT authorship contribution statement

Xu Zhang: Conceptualization, Methodology, Software, Validation, Formal analysis, Investigation, Resources, Data curation, Writing – original draft, Writing – review & editing, Visualization, Funding

acquisition. **Xiaoshan Fan:** Validation, Formal analysis, Resources, Data curation, Writing – review & editing, Supervision, Project administration.

Declaration of Competing Interest

The authors declare that they have no known competing financial interests or personal relationships that could have appeared to influence the work reported in this paper.

Acknowledgements

This work was financially supported by the National Natural Science Foundation of China (Grant No.: 52103074), the Natural Science Foundation of Shanghai (Grant No.: 21ZR1402800), the Fundamental Research Funds for the Central Universities (Grant No.: 2232020D-11), and the China Postdoctoral Science Foundation (Grant No.: 2021M690597).

References

[1] U. Tritschler, S. Pearce, J. Gwyther, G.R. Whittell, I. Manners, 50th anniversary perspective: Functional nanoparticles from the solution self-assembly of block copolymers, Macromolecules 50 (9) (2017) 3439–3463.
[2] A.O. Moughton, M.A. Hillmyer, T.P. Lodge, Multicompartment block polymer micelles, Macromolecules 45 (1) (2012) 2–19.
[3] J. Liu, Y. Ding, X. Liu, S. Lin, Q. Zhuang, Self-assembly of tunable ABC miktoarm terpolymers with semi-fluorinated segment for the discovery of a rich diversity of multicompartment micelles, Eur. Polym. J. 118 (2019) 465–473.
[4] X. Liu, Y. Ding, J. Liu, S. Lin, Q. Zhuang, Evolution in the morphological behaviour of a series of fluorine-containing ABC miktoarm star terpolymers, Eur. Polym. J. 116 (2019) 342–351.
[5] R.K. Raya, M. Štěpánek, Z. Limpouchová, K. Procházka, M. Svoboda, M. Lísal, E. Pavlova, A. Skandalis, S. Pispas, Onion micelles with an interpolyelectrolyte complex middle layer: Experimental motivation and computer study, Macromolecules 53 (16) (2020) 6780–6795.
[6] Y. Gan, Z.-D. Wang, Z.-X. Lu, Y. Shi, H.-Y. Tan, C.-F. Yan, Control on the morphology of ABA amphiphilic triblock copolymer micelles in dioxane/water mixture solvent, Chinese J. Polym. Sci. 36 (6) (2018) 728–735.
[7] T. Jiang, L. Wang, S. Lin, J. Lin, Y. Li, Structural evolution of multicompartment micelles self-assembled from linear ABC triblock copolymer in selective solvents, Langmuir 27 (2011) 6440–6448.
[8] D.-Y. Wang, H.-K. Liu, W. Wang, Chiral functional composites with broadening absorption and Modulatable Cotton effect, Compos. Commun. 27 (2021), 100859.
[9] X.-R. Feng, J.-X. Ding, R. Gref, X.-S. Chen, Poly(*β*-cyclodextrin)-mediated polylactide-cholesterol stereocomplex micelles for controlled drug delivery, Chinese J. Polym. Sci. 35 (6) (2017) 693–699.
[10] Z.G. Workineh, G. Pellicane, M. Tsige, Tuning solvent quality induces morphological phase transitions in miktoarm star polymer films, Macromolecules 53 (15) (2020) 6151–6162.
[11] J.-J. Fan, Y.-Y. Han, J. Cui, Solvent property induced morphological changes of ABA amphiphilic triblock copolymer micelles in dilute solution: A self-consistent field simulation study, Chinese J. Polym. Sci. 32 (12) (2014) 1704–1713.
[12] E.J. Cornel, J. Jiang, S. Chen, J.Z. Du, Principles and characteristics of polymerization-induced self-assembly with various polymerization techniques, CCS Chem. 2 (2020) 2104–2125.
[13] C.P. Callaway, N. Bond, K. Hendrickson, S.M. Lee, S.S. Jang, Structural tunability of multicompartment micelles as a function of lipophilic-fluorophilic block length ratio, J. Phys. Chem. B 122 (50) (2018) 12164–12172.
[14] Y. Lu, L. Gao, J. Lin, L. Wang, L. Zhang, C. Cai, Supramolecular step-growth polymerization kinetics of pre-assembled triblock copolymer micelles, Poly. Chem. 10 (2019) 3461–3468.
[15] J. Cui, W. Jiang, Simulation study of co-assembly of ABC triblock copolymer/nanoparticle into multicompartment hybrids in selective solvent, Chinese J. Polym. Sci. 31 (9) (2013) 1225–1232.
[16] Y.-C. Hsu, C.-I. Huang, W. Li, F. Qiu, A.-C. Shi, Micellization of linear A-*b*-(B-*alt*-C)$_n$ multiblock terpolymers in A-selective solvents, Polymer 54 (1) (2013) 431–439.
[17] S. Lin, F. Wang, J.Z. Du, High-genus multicompartment vesicles evolved from large compound micelles, Polym. Chem. 12 (2021) 3362–3366.
[18] T.-L. Nghiem, T. Chakroun, N. Janoszka, C. Chen, K. Klein, C.K. Wong, A. H. Groschel, pH-controlled hierarchical assembly/disassembly of multicompartment micelles in water, Macromol. Rapid Commun. 41 (18) (2020) 2000301.
[19] Q. Liu, X. Wang, L. Ma, K. Yu, W. Xiong, X. Lu, Y. Cai, Polymerization-induced hierarchical electrostatic self-assembly: Scalable synthesis of multicompartment polyion complex micelles and their monolayer colloidal nanosheets and nanocages, ACS Macro Lett. 9 (4) (2020) 454–458.
[20] S. Song, M. Puzhitsky, S. Ye, M. Abtahi, C.K. Rastogi, E. Lu, G. Hicks, I. Manners, M. A. Winnik, Crystallization-driven self-assembly of amphiphilic triblock terpolymers with two corona-forming blocks of distinct hydrophilicities, Macromolecules 53 (15) (2020) 6576–6588.
[21] X. Yue, Z. Geng, N. Yan, W. Jiang, Hierarchical self-assembly of a PS-b-P4VP/PS-b-PNIPAM mixture into multicompartment micelles and their response to two-dimensional confinement, PCCP 22 (3) (2020) 1194–1203.
[22] M. Wu, Y.T. Zhu, W. Jiang, Disassembly of multicompartment polymer micelles in spatial sequence using an electrostatic field and its application for release in chronological order, Angew. Chem.-Int. Edit. 57 (14) (2018) 3578–3582.
[23] Y.-C. Wu, B.P. Bastakoti, M. Pramanik, Y. Yamauchi, S.-W. Kuo, Multiple hydrogen bonding mediates the formation of multicompartment micelles and hierarchical self-assembled structures from pseudo A-*block*-(B-*graft*-C) terpolymers, Polym. Chem. 6 (2015) 5110–5124.
[24] J. Xia, D. Liu, C. Zhong, Multicompartment micelles and vesicles from π-shaped ABC block copolymers: a dissipative particle dynamics study, PCCP 9 (2007) 5267–5273.
[25] J. Xia, C. Zhong, Multicompartment micelles from π-shaped ABC block copolymers, Chin. J. Chem . 25 (11) (2007) 1732–1738.
[26] W. Wang, J. Zhang, C. Li, P. Huang, S. Gao, S. Han, A. Dong, D. Kong, Facile access to cytocompatible multicompartment micelles with adjustable Janus-cores from A-*block*-B-*graft*-C terpolymers prepared by combination of ROP and ATRP, Colloid Surf. B-Biointerfaces 115 (2014) 302–309.
[27] Y. Zhao, Y.-T. Liu, Z.-Y. Lu, C.-C. Sun, Effect of molecular architecture on the morphology diversity of the multicompartment micelles: A dissipative particle dynamics simulation study, Polymer 49 (22) (2008) 4899–4909.
[28] F. Shen, H. Ling, W. Ge, Y. Yang, X. Wang, J. Ren, X. Wang, Self-assembly behavior and conformation of amphiphilic hemicellulose-graft-fatty acid micelles, Carbohydr. Polym. 261 (2021), 117886.
[29] J. Zhang, Z.K. Wang, X.H. Wang, Z.G. Wang, The synthesis of bottlebrush cellulose-graft-diblock copolymer elastomers via atom transfer radical polymerization utilizing a halide exchange technique, Chem. Comm. 55 (2019) 13904–13907.
[30] J. Zhang, A.N. Keith, S.S. Sheiko, X. Wang, Z.G. Wang, To mimic mechanical properties of the skin by inducing oriented nanofiber microstructures in bottlebrush cellulose-*graft*-diblock copolymer elastomers, ACS Appl. Mater. Interfaces 13 (2021) 3278–3286.
[31] X.u. Zhang, J. Wang, Controllable interfacial adhesion behaviors of polymer-on-polymer surfaces during fused deposition modeling 3D printing process, Chem. Phys. Lett. 739 (2020) 136959, https://doi.org/10.1016/j.cplett.2019.136959.
[32] J. Wang, Y. Li, L. Zheng, L. Wu, H. Wang, X.u. Zhang, Self-assembly behaviors of graft copolymer structured fluid droplets on flat solid surfaces, Chem. Phys. Lett. 721 (2019) 43–48.
[33] J. Wang, Y. Li, L. Zheng, H. Wang, L. Wu, X.u. Zhang, Morphology transformation of micelles self-assembled from amphiphilic coil-coil diblock copolymer/nanoparticle mixture in dilute solution by combining self-consistent field theory and density functional theory, Chem. Phys. Lett. 710 (2018) 215–220.
[34] K. Ma, K.A. Spoth, Y. Cong, D. Zhang, T. Aubert, M.Z. Kurker, L.F. Kourkoutis, E. Mendes, U. Wiesner, Early formation pathways of surfactant micelle directed ultrasmall silica ring and cage structures, J. Am. Chem. Soc. 140 (50) (2018) 17343–17348.